AIP Journal of Applied Physics

Lead-free piezoceramics with giant strain in the system Bi 0.5 Na 0.5 Ti O 3 – Ba Ti O 3 – K 0.5 Na 0.5 Nb O 3 . I. Structure and room temperature properties

Shan-Tao Zhang, Alain Brice Kounga, Emil Aulbach, Torsten Granzow, Wook Jo, Hans-Joachim Kleebe, and Jürgen Rödel

Citation: Journal of Applied Physics **103**, 034107 (2008); doi: 10.1063/1.2838472

View online: http://dx.doi.org/10.1063/1.2838472

View Table of Contents: http://scitation.aip.org/content/aip/journal/jap/103/3?ver=pdfcov

Published by the AIP Publishing

Lead-free piezoceramics with giant strain in the system $Bi_{0.5}Na_{0.5}TiO_3-BaTiO_3-K_{0.5}Na_{0.5}NbO_3$. I. Structure and room temperature properties

Shan-Tao Zhang,[1] Alain Brice Kounga,[1] Emil Aulbach,[1] Torsten Granzow,[1] Wook Jo,[1,a)] Hans-Joachim Kleebe,[1] and Jürgen Rödel[1]
[1]*Institute of Materials Science, Technische Universität Darmstadt, Petersenstr. 23, 64287 Darmstadt, Germany*

(Received 10 September 2007; accepted 2 December 2007; published online 12 February 2008)

Lead-free piezoelectric ceramics, $(1-x-y)Bi_{0.5}Na_{0.5}TiO_3-xBaTiO_3-yK_{0.5}Na_{0.5}NbO_3$ ($0.05 \leqslant x \leqslant 0.07$ and $0.01 \leqslant y \leqslant 0.03$), have been synthesized by a conventional solid state sintering method. The room temperature ferroelectric and piezoelectric properties of these ceramics were studied. Based on the measured properties, the ceramics were categorized into two groups: group I compositions having dominant ferroelectric order and group II compositions displaying mixed ferroelectric and antiferroelectric properties at room temperature. A composition from group II near the boundary between these two groups exhibited a strain as large as ~0.45% at an electric field of 8 kV/mm. Polarization in this composition was not stable in that the piezoelectric coefficient d_{33} at zero electric field was only about 30 pm/V. The converse piezoelectric response becomes weaker when the composition deviated from the boundary between the groups toward either the ferroelectric or antiferroelectric compositions. These results were rationalized based on a field induced antiferroelectric-ferroelectric phase transition. © *2008 American Institute of Physics*. [DOI: 10.1063/1.2838472]

I. INTRODUCTION

Due to their excellent piezoelectric properties, lead-containing ceramics such as lead-zirconate-titanate ($Pb(Zr,Ti)O_3$) (PZT) or lead-magnesium-niobate–lead-titanate based solid solutions with perovskite structure have long been the materials of choice for piezoelectric sensor and actuator applications.[1] The performance of these devices is mainly governed by the electric field induced strain of the piezoelectric materials.[2] Up to now, Pb-based piezoelectric ceramics, especially PZT, have dominated the market of piezoelectric actuators since they exhibit much higher strain than their lead-free counterparts. However, environmental issues call for the use of nonhazardous substances for device fabrication, making the replacement of lead-containing ceramics imperative. Therefore, considerable effort has been devoted to the development of lead-free piezoceramics with properties comparable to PZT.

The high strain that can be obtained in PZT and related systems is generally attributed to two facts. First, the peculiar electronic structure of the Pb^{2+}-ion makes it highly polarizable, resulting in a large distortion of the crystal lattice. Second, the existence of a morphotropic phase boundary (MPB) between phases belonging to different crystal classes creates more degrees of freedom for ferroelectric domain orientation, also resulting in a higher piezoelectric effect. Consequently, research activities have been mainly focused on the MPB-region of solid solution systems containing nontoxic ions with an electronic structure similar to Pb^{2+}; in most cases, Bi^{3+} has been the ion of choice. Thus, much work has been devoted to systems such as $Bi_{0.5}Na_{0.5}TiO_3$ (BNT) and $K_{0.5}Na_{0.5}NbO_3$ (KNN).[3–6] However, current lead-free piezoceramics do not deliver electric field induced strains as large as Pb-based ceramics.[7] Therefore, an alternative approach in searching for lead-free piezoceramics with high strain is warranted.

We note that in Pb-based antiferroelectric ceramics such as $(Pb,La)(Sn,Zr,Ti)O_3$ (PLSZT), high strain is obtainable as a result of a field induced transition from an antiferroelectric (AFE) to a ferroelectric (FE) phase.[8–12] In fact, the development of actuators based on ceramic materials which undergo such a phase transition under electric field has been of great interest in the past decade.[12–14] However, this approach to inducing high strain has not yet been considered for lead-free piezoceramics.

In the lead-free $(1-x)Bi_{0.5}Na_{0.5}TiO_3-xBaTiO_3$ (BNT-BT) piezoelectric system, single crystals grown near the MPB composition (~0.94BNT-0.06BT) (Ref. 15) feature an electric-field dependent strain akin to antiferroelectric PLSZT solid solutions, which indicates the presence of an electric field induced AFE-FE phase transition.[16] On the other hand, it is known that doping can disrupt the long range ferroelectric order and lead to the formation and stabilization of the antiferroelectric order.[12] Based on these facts, we recently developed a lead-free $(0.94-x)$BNT-0.06BT-xKNN piezoceramic system by starting from 0.94BNT-0.06BT and substituting small amounts of the rhombohedral BNT with orthorhombic KNN. Throughout the present report, this system is referred to as BNT-BT-KNN. As shown in Ref. 17, introduction of only 2% KNN significantly changes the structure and properties of BNT-BT. At room temperature, this composition delivers an

a)Author to whom correspondence should be addressed. Electronic mail: jo@ceramics.tu-darmstadt.de.

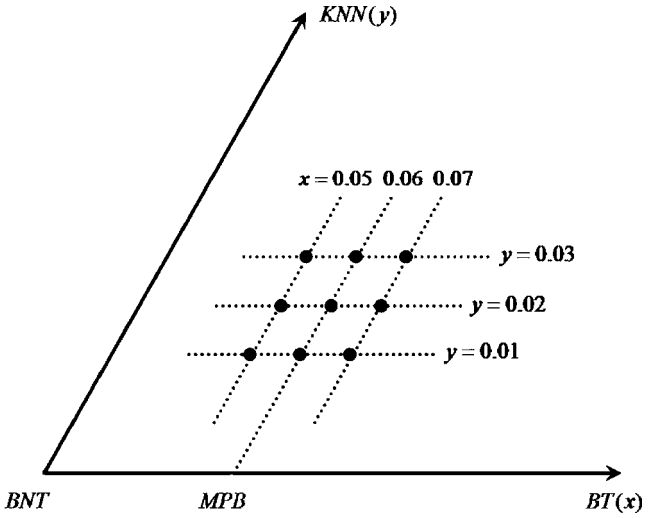

FIG. 1. The composition map of $(1-x-y)Bi_{0.5}Na_{0.5}TiO_3-xBaTiO_3-yK_{0.5}Na_{0.5}NbO_3$, $0.05 \leqslant x \leqslant 0.07$ and $0.01 \leqslant y \leqslant 0.03$, in the ternary lead-free system.

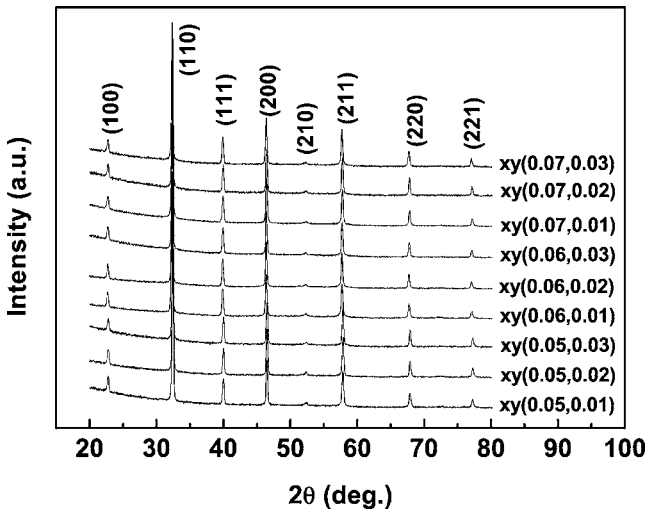

FIG. 2. X-ray diffractograms of all $(1-x-y)$BNT$-x$BT$-y$KNN samples. All compositions have single phase perovskite structure; there is no indication of a distortion in the cubic perovskite lattice.

electric-field induced strain as large as ~0.45% at an electric field of 8 kV/mm, which was proposed to be related to an electric field induced AFE-FE phase transition.[17] In this work, structures and properties of the compositions around 0.92BNT-0.06BT-0.02KNN were investigated in detail to understand the origin of the large strain and find the optimum composition for high-strain applications. For this purpose, ceramics with the stoichiometric formula of $(1-x-y)$BNT-xBT-yKNN, where $0.05 \leqslant x \leqslant 0.07$ and $0.01 \leqslant y \leqslant 0.03$ with steps of 0.01, were considered. The corresponding section of the phase diagram is shown in Fig. 1.

II. EXPERIMENTS

$(1-x-y)$BNT-xBT-yKNN ceramics were prepared by a conventional ceramic fabrication method using Bi_2O_3 (99.975%, Alfa Aesar), Na_2CO_3 (99.5%, Alfa Aesar), K_2CO_3 (99.0%, Alfa Aesar), $BaCO_3$ (99.8%, Alfa Aesar), TiO_2 (99.9%, Alfa Aesar), and Nb_2O_5 (99.9%, ChemPur) as starting raw materials. For each composition, the starting materials were weighed according to the stoichiometric formula and ball milled for 24 h in ethanol. The dried slurries were calcined at 900 °C for 3 h and then ball milled again for 24 h. The powders were subsequently pressed into green disks with a diameter of 10 mm under 70 MPa. Using a heating rate of 5 °C/min, sintering was carried out at 1100 °C for 3 h in covered alumina crucibles. To minimize the evaporation of the volatile elements Bi, Na, and K, the disks were embedded in a powder of the same composition.

The relative density of all samples was determined by the Archimedes method. The crystal structures of the ceramics were characterized by powder x-ray diffraction (STOE STADI P) using Cu $K\alpha_1$ radiation. Patterns were recorded on crushed unpoled sintered samples. For the microstructure determination, scanning electron microscopy (SEM) (XL 30 FEG, Philips) analyses were performed on polished and thermally etched (900 °C for 45 min) sample surfaces. The preparation of transmission electron microscopy (TEM) specimens followed standard ceramographic techniques which include cutting, grinding, polishing, and dimpling in addition to Ar-ion thinning to perforation and light carbon coating to minimize charging under the incident electron beam. TEM foils were characterized with a CM200 microscope (FEI Eindhoven, The Netherlands) operating at 200 keV. For comparison to the BNT-BT system, some materials for TEM investigations were also prepared without KNN.

Electric measurements were carried out on polished sintered disks with the thickness of ~0.5 mm. The circular surfaces of the disks were electroded with a thin layer of silver paste and fired at 550 °C for 30 min. Dielectric permittivity

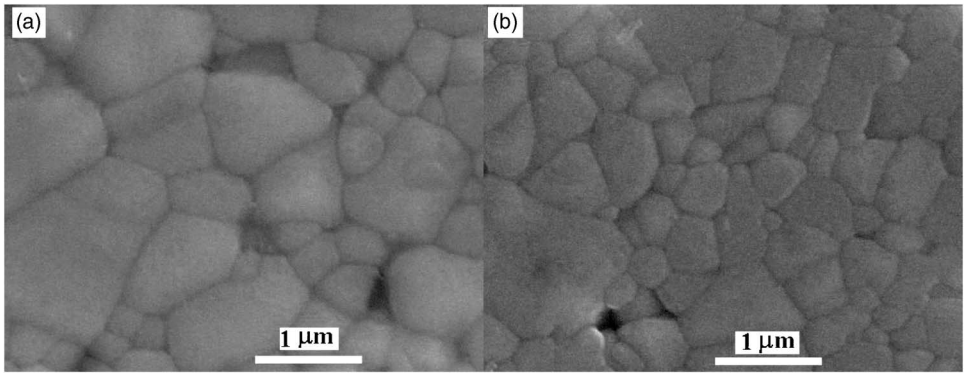

FIG. 3. SEM microstructures of (a) 0.93BNT-0.05BT-0.02KNN and (b) 0.91BNT-0.07BT-0.02KNN, showing dense homogeneous microstructure.

TABLE I. The summary of structure and property parameters of the BNT-BT-KNN lead free piezoceramics.

Composition (x,y)	Density (%)	Grain size (μm)	E_c (kV/mm)	P_r (μC/cm^2)	ε_r	tan δ
(0.05, 0.01)	98.3	1.0	3.2	38	2030	0.050
(0.05, 0.02)	98.3	1.0	3.1	32	2060	0.054
(0.05, 0.03)	98.2	1.0	1.9	30	2315	0.058
(0.06, 0.01)	98.6	1.0	1.4	31	2105	0.058
(0.06, 0.02)	98.6	1.0	1.3	16	2320	0.062
(0.06, 0.03)	98.1	0.9	0.9	12	2080	0.064
(0.07, 0.01)	98.5	0.8	0.8	8	1990	0.096
(0.07, 0.02)	98.5	0.8	1.0	11	2440	0.069
(0.07, 0.03)	99.1	0.9	1.2	14	2095	0.066
	Bipolar stain (%)	Negative strain (%)	Unipolar strain (%)	S_{max}/E_{max} (pm/V)	d_{33} (pm/V)	k_p
(0.05, 0.01)	0.29	0.13	0.21	269	90	0.24
(0.05, 0.02)	0.29	0.12	0.22	276	98	0.27
(0.05, 0.03)	0.41	0.11	0.28	346	70	0.19
(0.06, 0.01)	0.42	0.13	0.24	300	85	0.22
(0.06, 0.02)	0.45	0.045	0.45	567	30	···
(0.06, 0.03)	0.42	0.025	0.44	543	13	···
(0.07, 0.01)	0.41	0.015	0.43	535	7	···
(0.07, 0.02)	0.36	0.014	0.38	469	10	···
(0.07, 0.03)	0.34	0.037	0.34	405	21	···

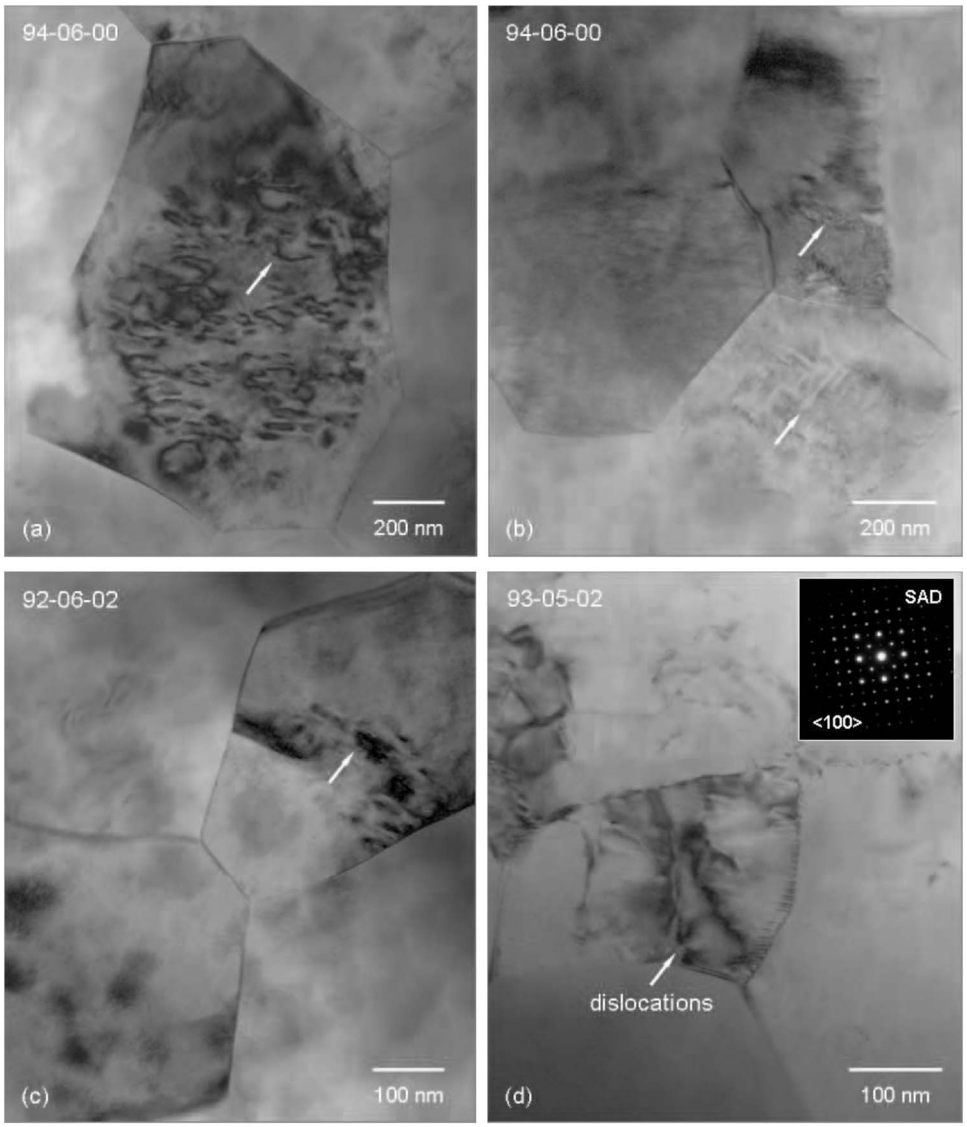

FIG. 4. TEM micrograph characteristic of the overall microstructure of the lead-free compositions studied.

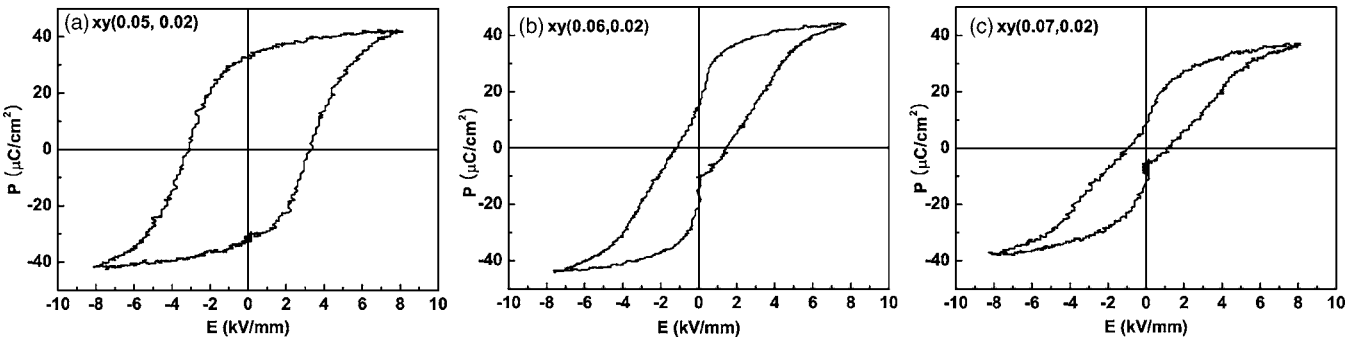

FIG. 5. The $P(E)$ hysteresis loops of (a) 0.93BNT-0.05BT-0.02KNN, (b) 0.92BNT-0.06BT-0.02KNN, and (c) 0.91BNT-0.07BT-0.02KNN. The loop becomes slim and pinched with increasing x, indicating the development of an antiferroelectric order.

and loss of unpoled ceramics were measured using an impedance analyzer (HP4284A, Hewlett-Packard Company) at frequencies ranging from 100 Hz to 1 MHz in a temperature range between 50 and 400 °C. The dependence of the polarization P and the longitudinal strain S on an alternating electric field E with an amplitude of 8 kV/mm was measured at a frequency of 50 mHz in a silicone oil bath with the aid of a Sawyer–Tower circuit and a linear variable differential transformer, respectively. A triangular waveform was chosen for the electric field cycle. A second set of samples was poled at room temperature by applying an electric field of 7 kV/mm for 5 min. The quasistatic piezoelectric coefficient d_{33} of these samples was measured using a Berlincourt-meter (YE 2730, SINOCERA), and the planar electromechanical coupling factor k_p was measured by a resonace-antiresonance method using an HP4192A impedance analyzer on the basis of IEEE standards.

III. RESULTS AND DISCUSSION

Figure 2 shows the x-ray diffraction (XRD) patterns of the $(1-x-y)$BNT-xBT-yKNN compositions. The patterns prove that all ceramics are crystallized into a single phase perovskite structure. No obvious change in the positions and relative intensities of all reflections was observed, suggesting similar crystal structures for all compositions. All the peaks could be indexed based on a cubic perovskite structure because no splitting of any of the peaks was detected. In this regard, all compositions are thought to be similar to 0.92BNT-0.06BT-0.02KNN crystallographically.[17]

Dense and homogeneous microstructures were obtained in all compositions. Figure 3 exemplarily shows SEM micrographs of 0.93BNT-0.05BT-0.02KNN and 0.91BNT-0.07BT-0.02KNN. The densities (between 98.1% and 99.1% of theoretical density) and the average grain size of all compositions are summarized in Table I. The average grain size is about 1 μm with little change with KNN content. Figure 4 displays a sequence of four TEM micrographs characteristic for the overall microstructure of the various compositions studied, including two samples without KNN content. All samples revealed a rather similar microstructure independent of a specific composition. Thus, the corresponding images shown in Fig. 4 are discussed together and not in relation to their position within the ternary phase diagram (cf. Fig. 1). Unexpectedly, none of the compositions studied revealed a distinct domain boundary contrast. No secondary phase present at triple grain junctions or along interfaces such as amorphous grain boundary films was observed. The overall microstructure of all samples is rather homogeneous and composed of a single phase material irrespective of composition, which is in agreement with the XRD data presented in Fig. 2. However, it is noted that individual grains of the different materials commonly show contrast variations related to the formation of intrinsic defects, as illustrated, for example, in Fig. 4(a). Figure 4(d) reveals the presence of

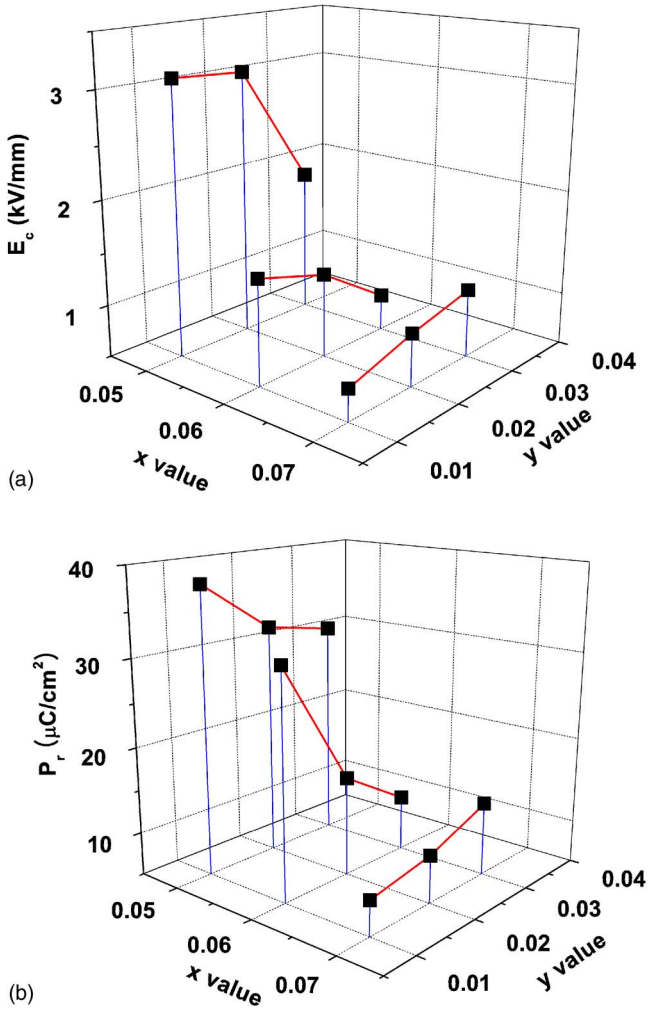

FIG. 6. (Color online) (a) Coercive field E_c and (b) remnant polarization P_r of each composition.

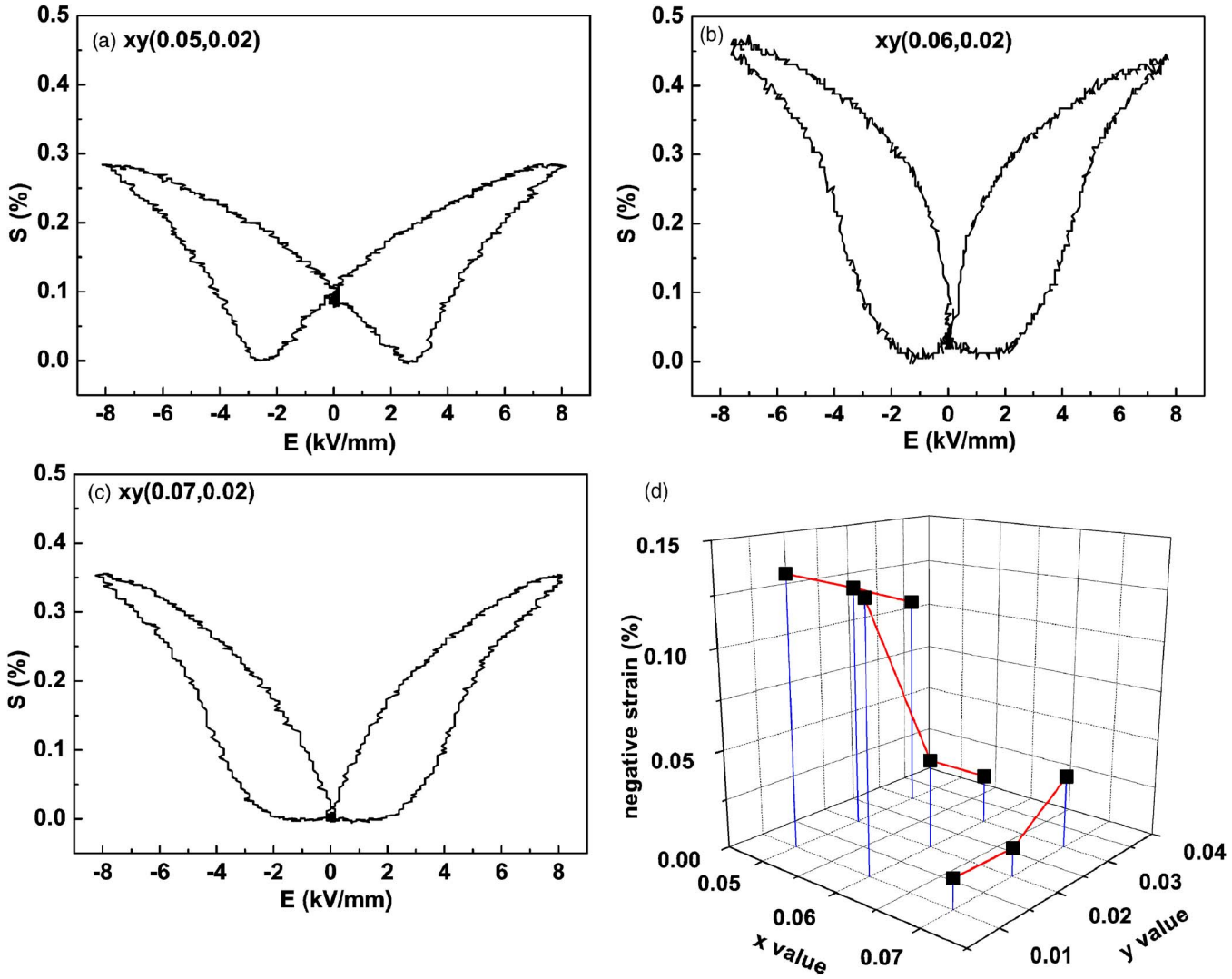

FIG. 7. (Color online) Bipolar $S(E)$ curves of (a) 0.93BNT-0.05BT-0.02KNN, (b) 0.092BNT-0.06BT-0.02KNN, and (c) 0.91BNT-0.07BT-0.02KNN. (d) Notice that the negative bipolar strain values gradually disappear with increasing x.

dislocations, which are thought to be introduced into the material during densification via locally high sintering stresses. These contrast features are far less prominent than the contrast variations depicted in Figs. 4(a) and 4(c). It is suggested that these local contrast variations represent intrinsic point defects such as the agglomeration of point defects, which also contribute to local deformation of the lattice, generating the observed contrast variations.

The $P(E)$ hysteresis loops of 0.93BNT-0.05BT-0.02KNN, 0.92BNT-0.06BT-0.02KNN, and 0.91BNT-0.07BT-0.02KNN are depicted in Figs. 5(a)–5(c). With increasing x, the loop became slim, characterized by a significantly reduced coercive field (E_c) and remnant polarization (P_r). The loops appear "pinched," which is a characteristic feature of antiferroelectric materials. The values of E_c and P_r are shown in Table I and displayed in a three-dimensional plot in Fig. 6. These data suggest that there are two different compositional regions which can be separated by a boundary line approximately connecting the compositions 0.92BNT-0.05BT-0.03KNN and 0.93BNT-0.06BT-0.01KNN in Fig. 1. Compositions on the left side of or on this line, i.e., 0.94BNT-0.05BT-0.01KNN, 0.93BNT-0.05BT-0.02KNN, 0.92BNT-0.05BT-0.03KNN, and 0.93BNT-0.06BT-0.01KNN belong to group I. Ceramics from this group display predominantly ferroelectric behavior. Group II consists of the compositions on the right side of the line, i.e., 0.92BNT-0.06BT-0.02KNN, 0.91BNT-0.06BT-0.03KNN, 0.92BNT-0.07BT-0.01KNN, 0.91BNT-0.07BT-0.02KNN, and 0.90BNT-0.07BT-0.03KNN. These materials display properties commonly associated with antiferroelectrics, although there still are traces of ferroelectric behavior, such as a measurable remnant polarization and a piezoelectric coefficient d_{33}. We, therefore, suggest that these compositions simultaneously possess both ferroelectric and antiferroelectric orders at room temperature. We presume that the antiferroelectric order is metastable at room temperature.

The relative dielectric constant ε_r and dielectric loss $\tan\delta$ measured at 50 °C with a frequency of 10 kHz are given in Table I for all compositions. Neither of the values shows a systematic dependence on composition. ε_r was observed to vary in a range between 2000 and 2400, which is higher than that of KNN-based lead-free ceramics[4,7] and comparable to that of BNT-based lead-free ceramics.[18,19] $\tan\delta$ varied between 0.05 and 0.09.

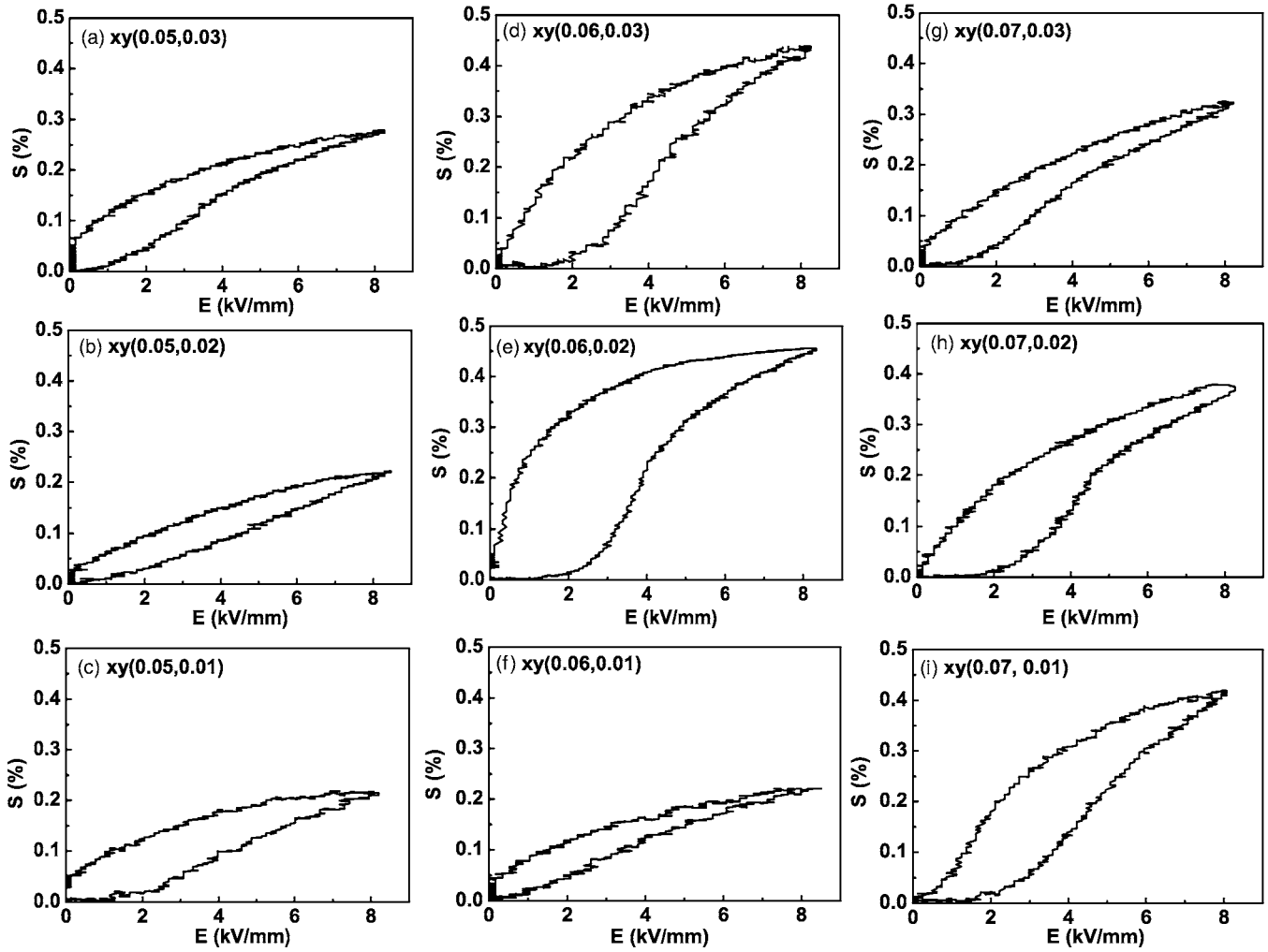

FIG. 8. Unipolar $S(E)$ curves of all compositions. Note the change of shape and maximum strain values between compositions of groups I and II.

Figure 7 displays the bipolar $S(E)$ curves of 0.93BNT-0.05BT-0.02KNN, 0.92BNT-0.06BT-0.02KNN, and 0.91BNT-0.07BT-0.02KNN measured at room temperature. The maximum strains of these three compositions were 0.29%, 0.45%, and 0.36%, respectively. 0.93BNT-0.05BT-0.02KNN, a representative of group I, showed a butterfly-shaped $S(E)$ curve, which is typical for ferroelectric materials.[16] The other compositions from the group I showed a similar shape of $S(E)$ loops. In contrast, group II compositions, which are displayed by the example of 0.92BNT-0.06BT-0.02KNN and 0.91BNT-0.07BT-0.02KNN, showed a different behavior: the strain disappeared on removal of the electric field, and no negative strain was observed when the polarization orientation was reversed. Again, this behavior is similar to that of ceramics with a dominant antiferroelectric order.[8–12,16] As a quantitative measurement on the shape change of the $S(E)$-curves, we plotted the "negative strain" (i.e., the difference between the zero-field strain and the lowest strain) for all compositions as shown in Fig. 7(d), which clearly shows the difference between groups I and II compositions.

To evaluate the suitability of the materials for actuator applications and to highlight the peculiarities of the studied materials, the strain response of the material under unipolar electric field cycling is plotted for all compositions, as shown in Fig. 8. Ceramics from group I generally showed comparably smaller hysteresis and a maximum strain of 0.22%–0.27%, while those of group II displayed more hysteretic behavior and had a higher maximum strain of 0.34%–0.45%. There is an apparent correlation between Fig. 7(d) (negative strain) and Fig. 8 (unipolar strain): A large negative strain reduces the potential for a material to display large strains upon unipolar electric loading. The detailed maximum strain values are shown in Table I. The highest strain of 0.45% was achieved in 0.92BNT-0.06BT-0.02KNN, whose composition lies next to the boundary. It should be noted that the strains observed in compositions of group II are the largest ever reported for polycrystalline lead-free ceramics and comparable to some Pb-based antiferroelectric ceramics.[17]

To put the strain values into perspective, the large signal d_{33}, i.e., the ratio S_{max}/E_{max}, where S_{max} denotes the maximum unipolar strain and E_{max} (=8 kV/mm) is the maximum electric field, is presented in Table I. It can be noted that for group I compositions, S_{max}/E_{max} varied in the range of 269–300 pm/V, whereas it ranged between 405 and 567 pm/V for group II materials. These values are even higher than those of untextured lead-containing polycrystalline ferroelectric ceramics.[17] At the same time, the small-

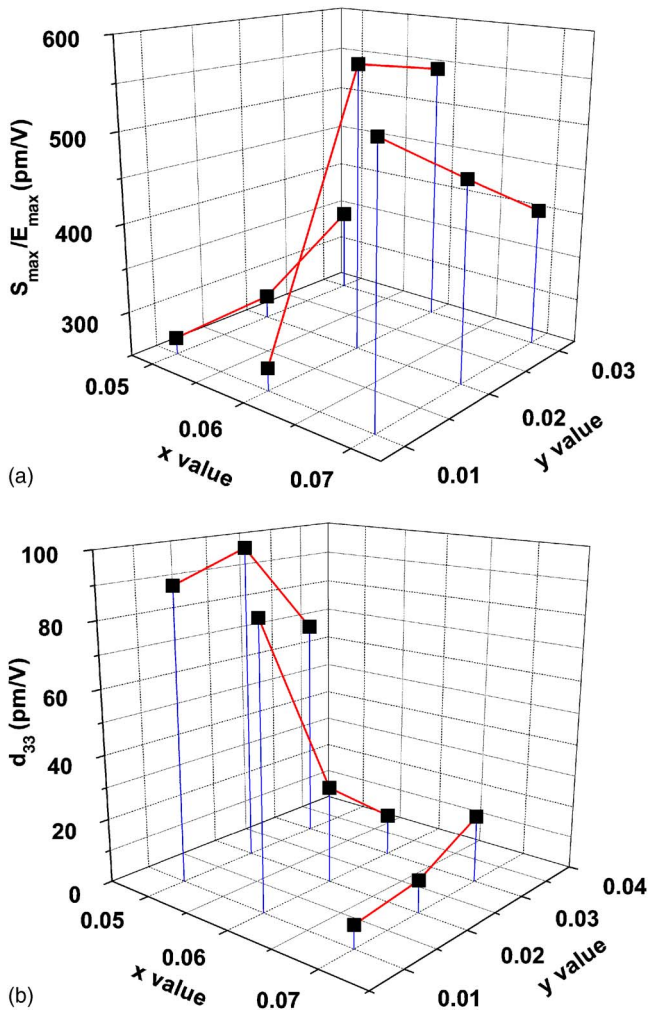

FIG. 9. (Color online) Three-dimensional plots of (a) S_{max}/E_{max} and (b) quasistatic d_{33}.

signal d_{33} values, which are also displayed in Table I as well as Fig. 9, were smaller for group II materials when compared with group I compositions or even with other reported lead-free ferroelectric materials.[3–7] This is not surprising, since the intrinsic piezoelectric and dielectric responses are related through the following equation:

$$d_{33} = 2\varepsilon_{33}\varepsilon_0 Q_{11} P_r, \tag{1}$$

where ε_0 is the vacuum permittivity. Group II compositions had a reduced remnant polarization by about a factor of 3 as compared with group I compositions. However, the permittivity near room temperature varied only by about 20% throughout all the compositions. Therefore, the low d_{33} values of group II can be attributed to the strong reduction in P_r. This reduced remnant polarization is consistent with the suggested dominant antiferroelectric order in group II compositions. Accordingly, the large strain measured in materials of this group can mostly be attributed to a field induced phase transition from antiferroelectric to ferroelectric order. This type of transition is generally reported to involve a structural change accompanied by a large volume change and a consequent large longitudinal strain. In this context it should be noted that the relevant parameter for the evaluation of a material's suitability for most actuator applications is not the zero-field small-signal d_{33} value, which is indeed quite small in any material with a predominant antiferroelectric ordering, but the total strain that can be obtained under a field, which can be very large due to the AFE-FE phase transition.

The electromechanical coupling factors k_p of the compositions of group I were summarized in Table I. The values were in the range of 0.19–0.27, which are comparable to those of other reported BNT-based lead-free piezoceramics.[7] The absence of k_p values for the compositions of group II is due to no or negligible resonance-antiresonance peaks observed.

Although KNN itself shows ferroelectric order, its addition into BNT-BT appears to disrupt the ferroelectric order of BNT-BT and leads to the development of an antiferroelectric order. This tendency becomes dominant in group II, leading to the observed decrease in P_r, E_c, and d_{33}. Similar to Pb-based antiferroelectric ceramics, the compositions of group II seem to derive most of their strain from an AFE-FE phase transition induced by the electric field. Since the strain at zero field is negligible, the strain reached under unipolar load is identical to that obtained during bipolar cycling.[10] We, therefore, believe that this material system offers a pathway for tailoring lead-free high-strain actuator materials based on a field induced AFE-FE phase transition.

However, we should point out that the large strain can only exist in compositions located in a narrow region where ferroelectric and antiferroelectric orders coexist and have the competitive free energy in the BNT-BT-KNN ternary phase diagram. Far away from this region, either the free energy of the ferroelectric or that of the antiferroelectric order will dominate. Each of these phases alone will not deliver a strain as large as that measured from the compositions close to the boundary because this strain results from the contributions both of domain switching and of field induced phase transition. Therefore, compositions with mostly ferroelectric order can only deliver a unipolar strain corresponding to the maximum piezoelectric coefficient of 98 pC/N. If, on the other hand, the composition is too far in the antiferroelectric phase, the field required to induce the transition into the ferroelectric phase might exceed the dielectric breakdown strength, impeding the development of large strain in the ceramic.

IV. SUMMARY

$(1-x-y)$BNT-xBT-yKNN $(0.05 \leqslant x \leqslant 0.07$ and $0.01 \leqslant y \leqslant 0.03)$ lead-free piezoceramics were synthesized and investigated at room temperature. Both x-ray and TEM investigations cannot reveal structural differences among the materials investigated, but suggest a cubic crystal structure, where consistently domains cannot be revealed during the TEM analyses. Piezoelectric measurements, however, suggest a classification into two groups: one with dominant ferroelectric order and the other with mixed ferroelectric and antiferroelectric ordering. The two groups showed markedly different shapes of the $P(E)$ and $S(E)$ hysteresis loops as well as E_c and P_r values. For compositions located near the boundary between the ferroelectric and antiferroelectric regions, a giant strain as high as 0.45% was attained under an electric field of 8 kV/mm. This giant strain was attributed to

a combination of the lattice volume change caused by a field-induced AFE-FE phase transition and ferroelectric domain reorientation. Our results suggest that the system BNT-BT-KNN is an environmentally friendly candidate material class for application in electromechanical devices and provides an alternative way in the quest for potential lead-free actuator materials.

This work was supported by the Deutsche Forschungsgemeinschaft (DFG) under SFB 595. S.T.Z. thanks the Alexander von Humboldt foundation for financial support. We acknowledge helpful support from M. Hinterstein for the structural analyses.

[1]G. H. Haertling, J. Am. Ceram. Soc. **82**, 797 (1999).
[2]S. E. Park and T. R. Shrout, J. Appl. Phys. **82**, 1804 (1997).
[3]Y. Saito, H. Takao, T. Tani, T. Nonoyama, K. Takator, T. Homma, T. Nagaya, and M. Nakamura, Nature (London) **432**, 84 (2004).
[4]E. Hollenstein, M. Davis, D. Damjanovic, and N. Setter, Appl. Phys. Lett. **87**, 182905 (2005).
[5]C. Ang, Z. Yu, Z. Jing, R. Guo, A. S. Bhalla, and L. E. Cross, Appl. Phys. Lett. **80**, 3424 (2002).
[6]S. J. Zhang, R. Xia, T. R. Shrout, Z. G. Zang, and J. F. Wang, J. Appl. Phys. **100**, 104108 (2006).
[7]S. Zhang, T. R. Shrout, H. Nagata, Y. Hiruma, and T. Takenaka, IEEE Trans. Ultrason. Ferroelectr. Freq. Control **54**, 910 (2007) and references therein.
[8]R. P. Brodeur, K. W. Gachigi, P. M. Pruna, and T. R. Shrout, J. Am. Ceram. Soc. **77**, 3042 (1994).
[9]S. E. Park, M. J. Pan, K. Markowski, S. Yoshikawa, and L. E. Cross, J. Appl. Phys. **82**, 1798 (1997).
[10]C. Heremanns and H. L. Tuller, J. Appl. Phys. **87**, 1458 (2000).
[11]Y. W. Nam and K. H. Yoon, Mater. Res. Bull. **36**, 171 (2001).
[12]Y. J. Yu and R. N. Singh, J. Appl. Phys. **94**, 7250 (2003).
[13]K. Uchino, *Piezoelectric Actuators and Ultrasonic Motors* (Kluwer Academic, Dordrecht, 1997).
[14]W. Y. Pan, W. Y. Gu, and L. E. Cross, Ferroelectrics **99**, 185 (1998).
[15]T. Takenaka, K. Maruyama, and K. Sakata, Jpn. J. Appl. Phys., Part 1 **30**, 2236 (1991).
[16]Y. M. Chiang, G. W. Farrey, and A. N. Soukhojak, Appl. Phys. Lett. **73**, 3683 (1998).
[17]S. T. Zhang, A. B. Kounga, E. Aulbach, H. Ehrenberg, and J. Rödel, Appl. Phys. Lett. **91**, 112906 (2007).
[18]T. Oh, Jpn. J. Appl. Phys., Part 1 **45**, 5138 (2006).
[19]Y. Hiruma, H. Nagata, and T. Takenaka, Jpn. J. Appl. Phys., Part 1 **45**, 7409 (2006).